Deriving the mean excitation energy map from DECT and pCT

Largely inspired by [Vilches-Freixas, Quiñones, Létang, and Rit, 2018]

Jean Michel Létang

pCT Workshop – June 15, 2018

Stopping power formula

The model of the collision stopping power from [Bethe, 1930]

$$S = 4\pi r_e^2 m_e c^2 \rho_e \frac{z^2}{\beta^2}\left[\ln \frac{2 m_e c^2 \beta^2 \gamma^2}{I} - \beta^2\right]$$

omitting shell, density-effect, Barkas and Bloch corrections.

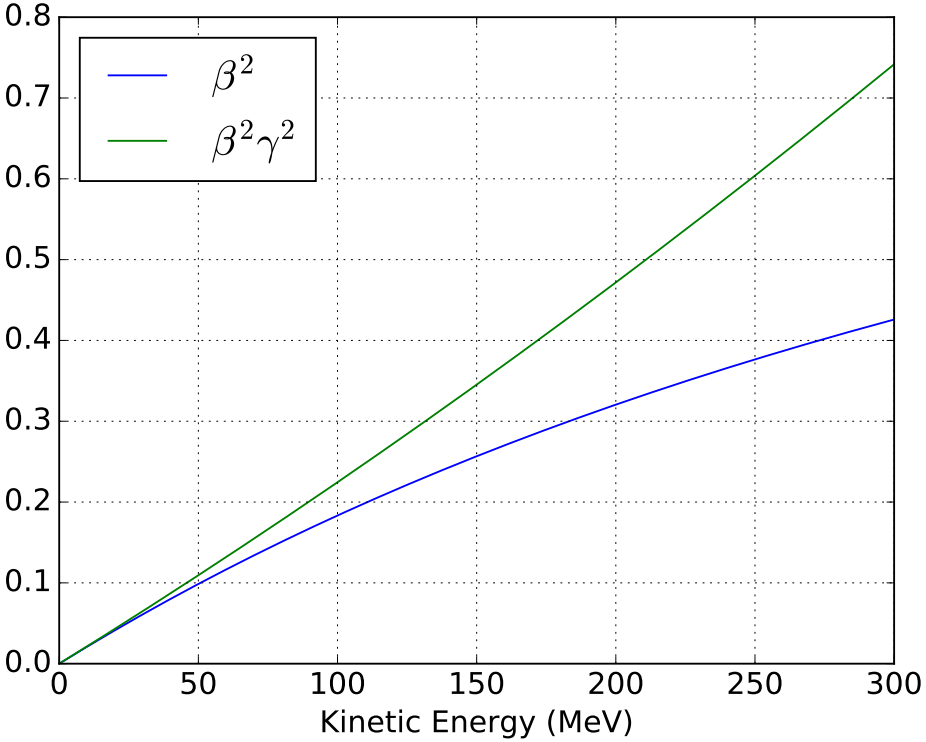

For protons:

$$\beta(E) = \frac{v}{c} = \sqrt{1 - \left(\frac{m_p c^2}{m_p c^2 + E}\right)^2}$$

$$\gamma(E) = 1 + \frac{E}{m_p c^2}$$

Stopping power dependence

[ICRU, 1993]

Logarithmic dependence of S vs I $\Rightarrow$ fine accuracy on I not required

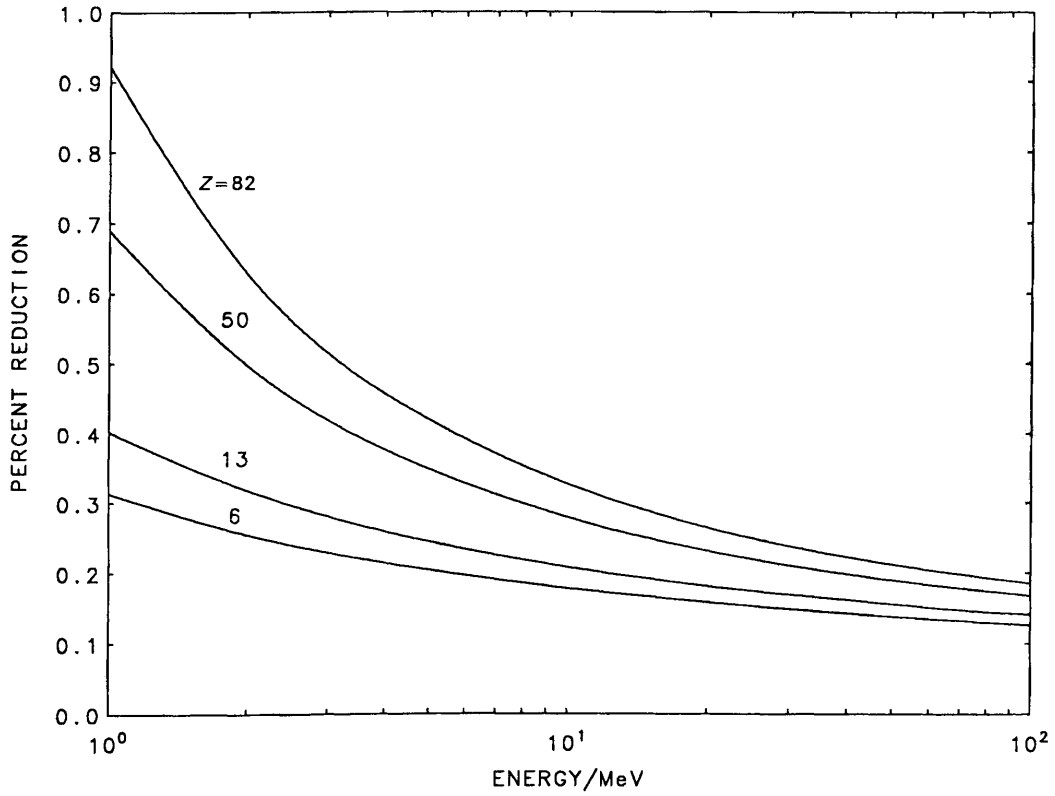

Percentage reduction of S for protons resulting from a 1% increase of I

Mean excitation energies for elements

[Tanabashi and PDG, 2018][ICRU, 1984][ICRU, 1993]

The mean excitation energy, I, is a quantity independent of the properties of the projectile, and depends only on the properties of the medium.

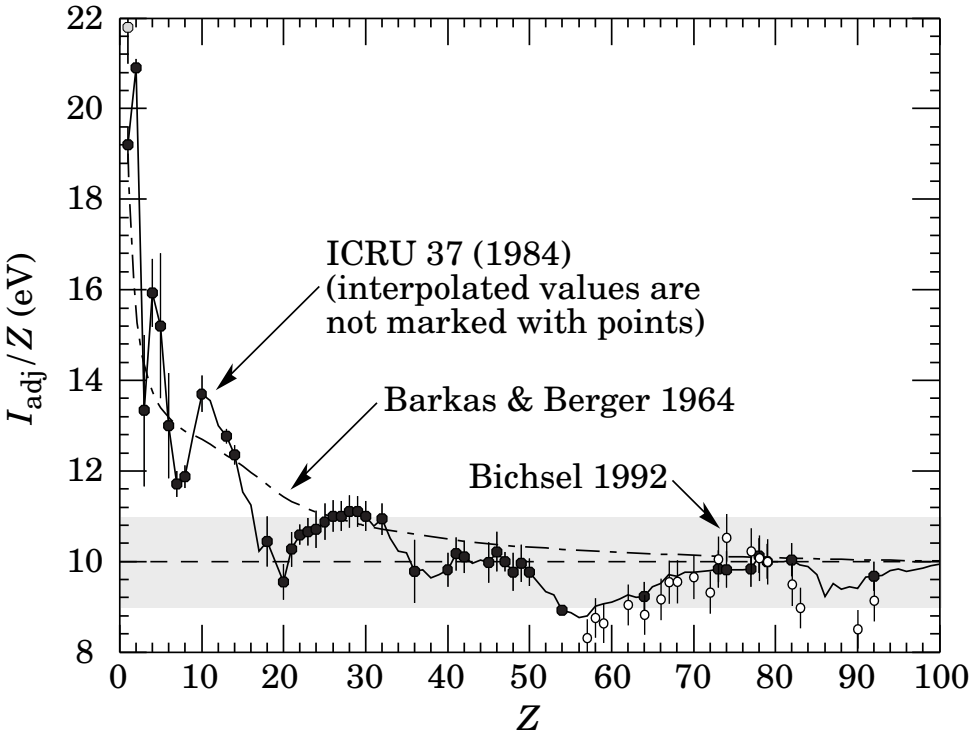

As shown by Bloch [1933] for the Thomas-Fermi model of the atom, $I \approx I_0 Z$, with I_0 approximately equal to 10 eV.

The most frequently applied method of obtaining I-values is to extract them from measured stopping powers or ranges, using a stopping-power formula.

Mean excitation energies for compounds

[ICRU, 1993]

"The determination of the mean excitation energy is the principal non-trivial task in the evaluation of the Bethe stopping-power formula."

[Seltzer and Berger, 1982]

In order to obtain an accurate estimate of the I-value, it is necessary to account for the specific electronic structure of the atom, molecule, or solid.

Bragg's additivity rule on mass collision stopping power for compound m

$$\left(\frac{S}{\rho}\right)_m = \sum_j \omega_j \left(\frac{S}{\rho}\right)_j \quad \xRightarrow{\text{Bethe}} \quad \ln I_m = \frac{\sum_j \omega_j \left(\frac{Z_j}{A_j}\right) \ln I_j}{\sum_j \omega_j \left(\frac{Z_j}{A_j}\right)}$$

with j sum over molecular fragments or functional groups for better accuracy

I-value of water

[Besemer et al., 2013][Sabin et al., 2013]

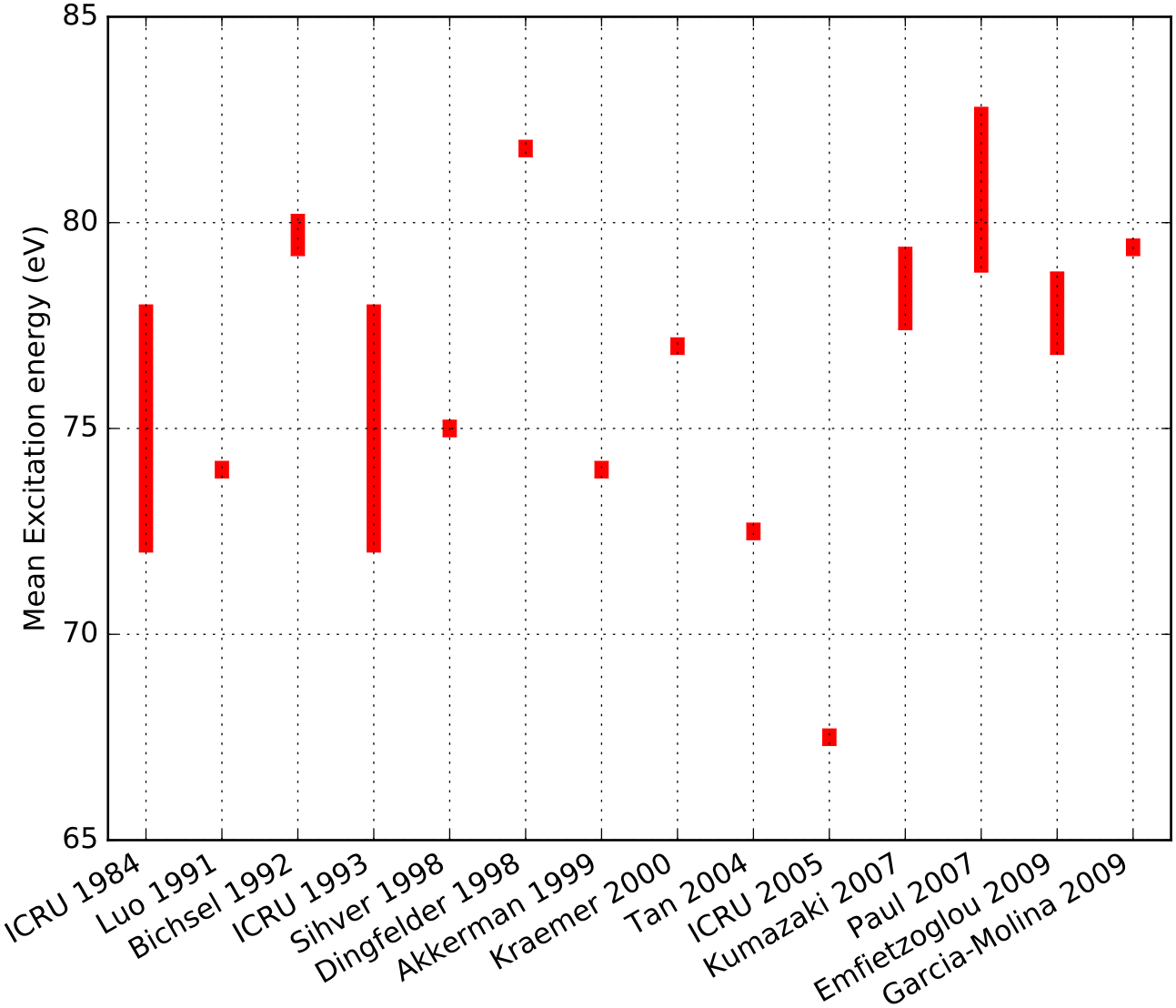

Even the determination of mean excitation energie of water is not a trivial task.

I-values for water range in $[67 : 82]$ eV $\equiv$ 18.5% uncertainty.

A generally accepted *I*-value for water has not been established yet.

Human tissue *I*-value

[Doolan et al., 2016]

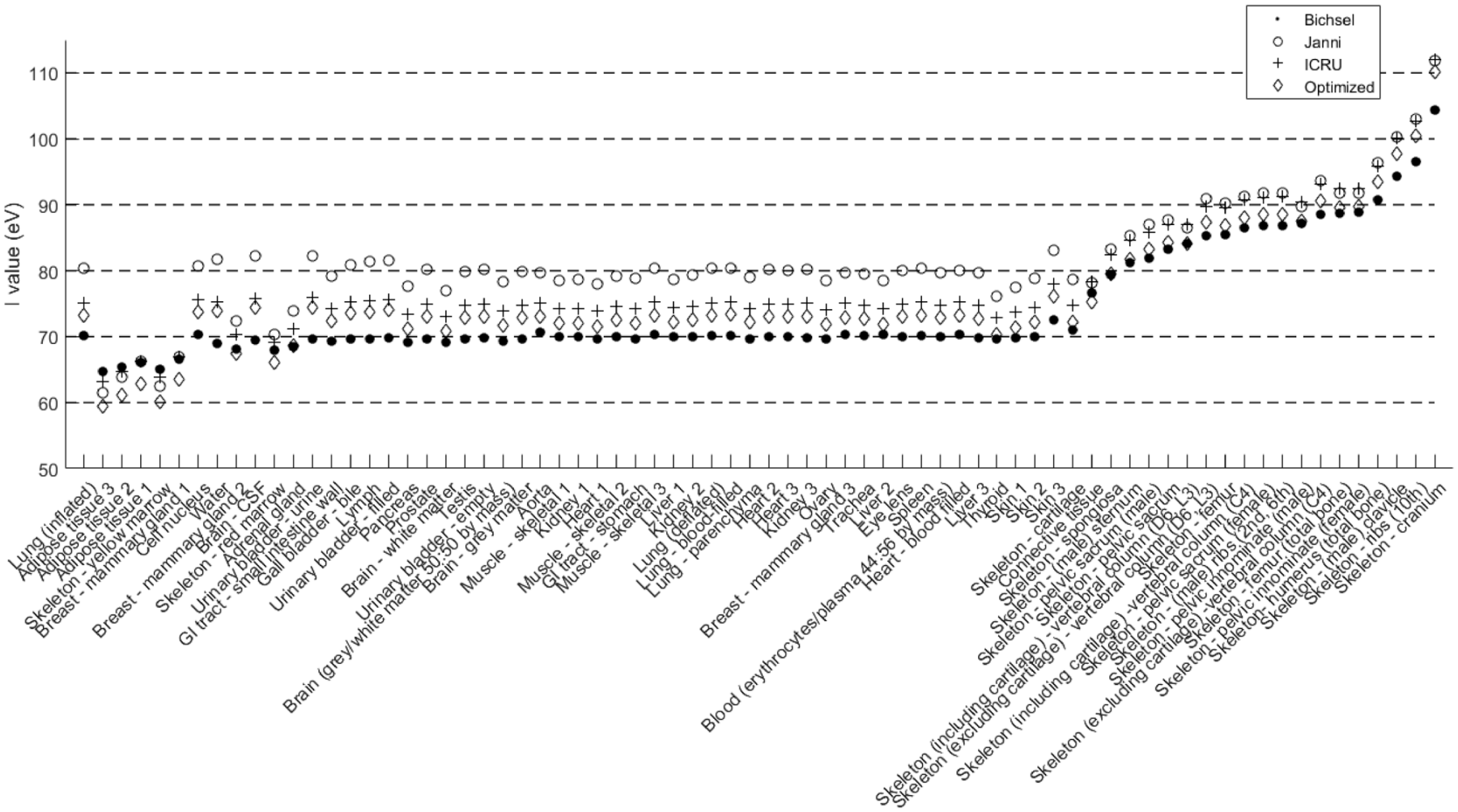

Impact of I-value uncertainty on range

[Besemer et al., 2013]

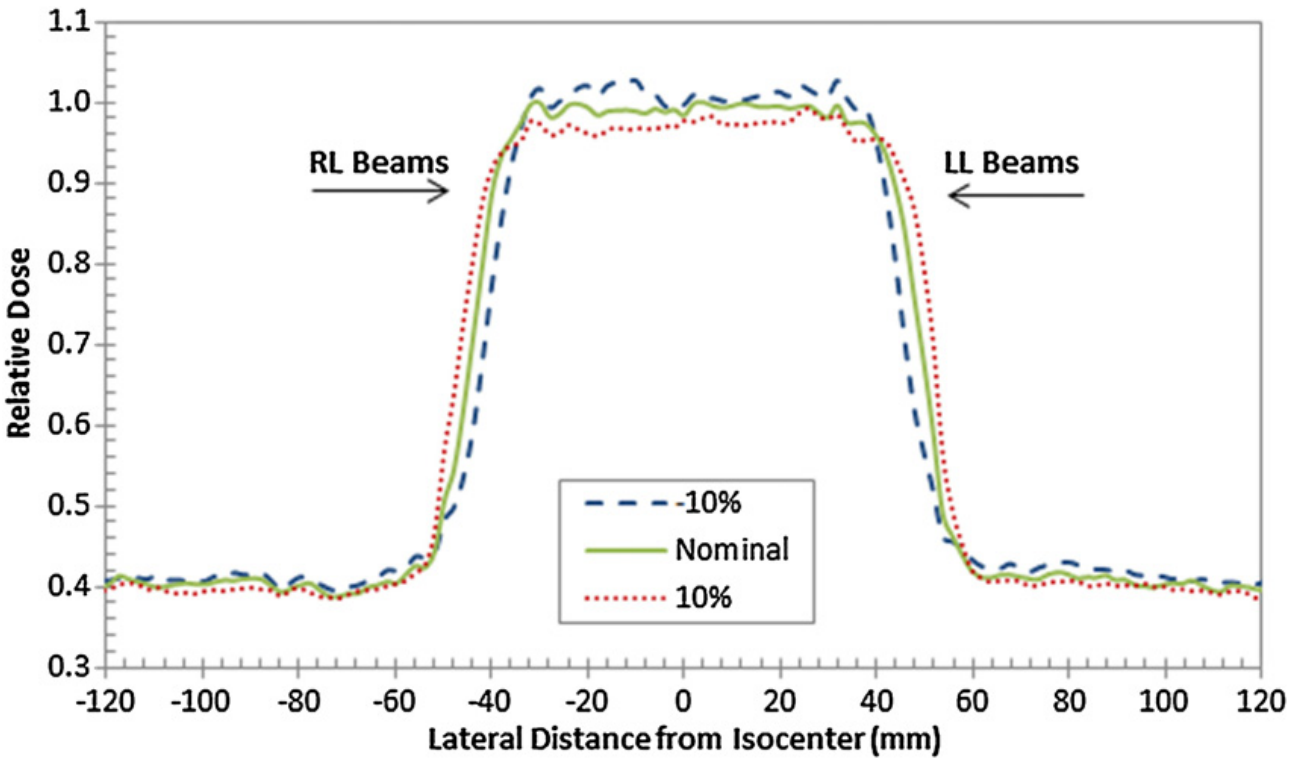

A lateral depth dose curve (SOBP) composed of two right lateral (RL) beams and two LL beams for the prostate patient.

Modulating the I-value up to $\pm 10\%$ the nominal value shifted the R_{90} range by up to 7.7 mm (2.7% of the range) from the nominal range.

Impact of *I*-value uncertainty on dose

[Besemer et al., 2013]

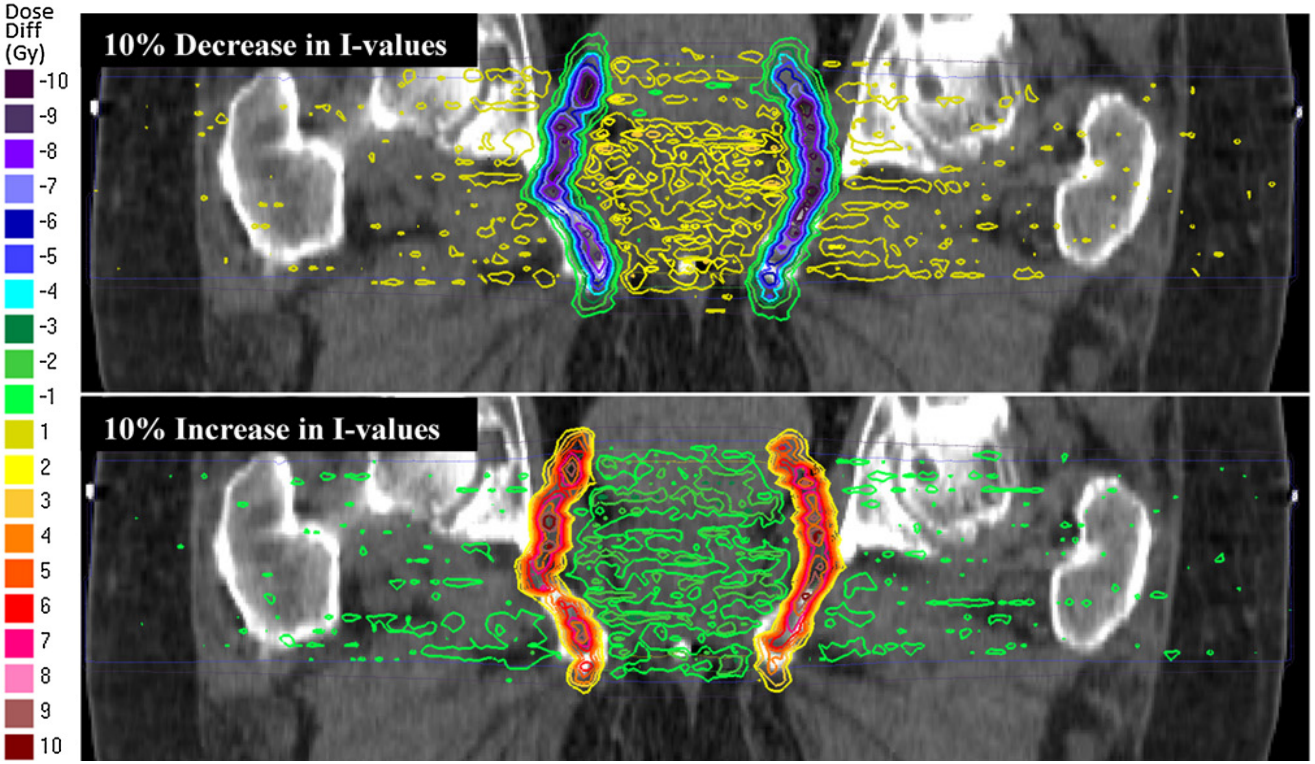

Isodose curves showing the dose difference between treatments with a 10% uniform decrease/increase in tissue *I*-values.

The range changes in the prostate patient resulted in two large dose gradients regions at the distal edges of the beams where the dose differs from the nominal case by larger than ± 9 Gy in some regions.

Estimation of I

DECT - pCT combination

Doolan et al. [2016] showed that ignoring many of the corrections in Bethe's formulation, as first proposed by Schneider et al. [1996] using optimized I-values (fitted to measurements of Gammex insert RSPs), has the lowest errors in determining the RSP.

$$S = 4\pi r_e^2 m_e c^2 \rho_e \frac{z^2}{\beta^2}\left[\ln\frac{2m_e c^2\beta^2\gamma^2}{I} - \beta^2\right]$$

$$\frac{S}{S_{\text{water}}} = \text{RSP} = \frac{\rho_{e,\text{m}}}{\rho_{e,\text{water}}}\left[\ln\frac{2m_e c^2\beta^2\gamma^2}{I} - \beta^2\right] \Big/ \left[\ln\frac{2m_e c^2\beta^2\gamma^2}{I_w} - \beta^2\right]$$

$$\frac{\rho_e}{\rho_{e,\text{water}}} = \text{RED}$$

$$I(\boldsymbol{x}) = 2m_e c^2\beta^2\gamma^2 \exp\left(-\frac{\text{RSP}(\boldsymbol{x})}{\text{RED}(\boldsymbol{x})}\left[\ln\frac{2m_e c^2\beta^2\gamma^2}{I_{\text{w}}} - \beta^2\right] - \beta^2\right)$$

Two problems: estimate RSP and RED

Estimation of the RSP: pCT

[Arbor et al., 2015][Rit et al., 2015]

Along the proton path P with curvilinear abscissa p

$$\mathrm{WEPL} \equiv \int_{E_{\mathrm{in}}}^{E_{\mathrm{out}}} \frac{1}{S_{\mathrm{water}}(E)} \mathrm{d}E = \int_{E_{\mathrm{in}}}^{E_{\mathrm{out}}} \frac{S(E)}{S_{\mathrm{water}}(E)} \frac{\mathrm{d}E}{S(E)} \approx \int_{p \in P} \mathrm{RSP}(p)\, \mathrm{d}p$$

assuming that $\mathrm{RSP} = S(E)/S_{\mathrm{water}}(E)$ of a material does not on E.

$$\Downarrow$$

Direct reconstruction of the RSP via Radon transform applied to the proton MLP

Estimation of the RSP: proton energy dependence

[Arbor et al., 2015]

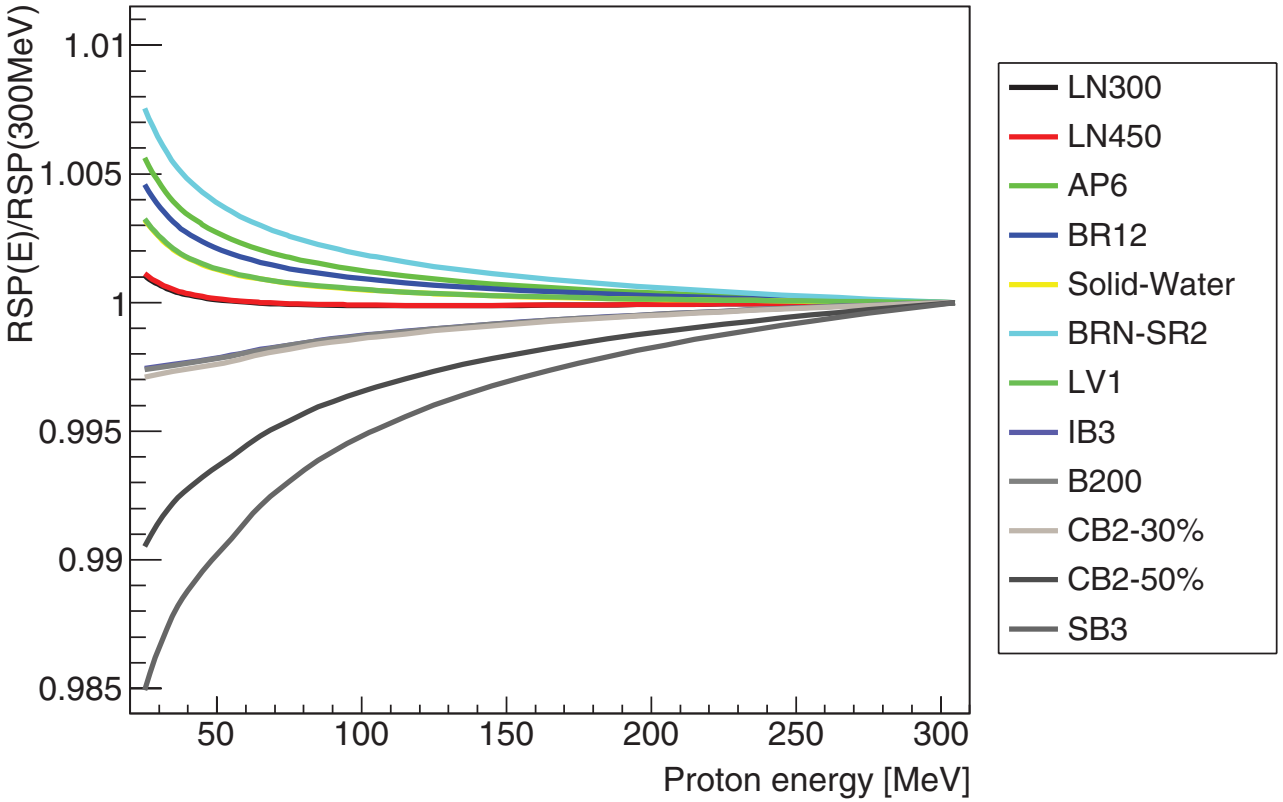

Geant4 relative stopping power of Gammex 467 materials, divided by the 300 MeV value, as a function of the proton energy.

The proton stopping power relative to the proton stopping power of water is constant with the proton energy within less than 0.7% variations for Gammex 467 materials in the 80 – 300 MeV energy range.

Estimation of the RSP: deviation

[Arbor et al., 2015]

p@300 MeV – 1mGy imaging dose

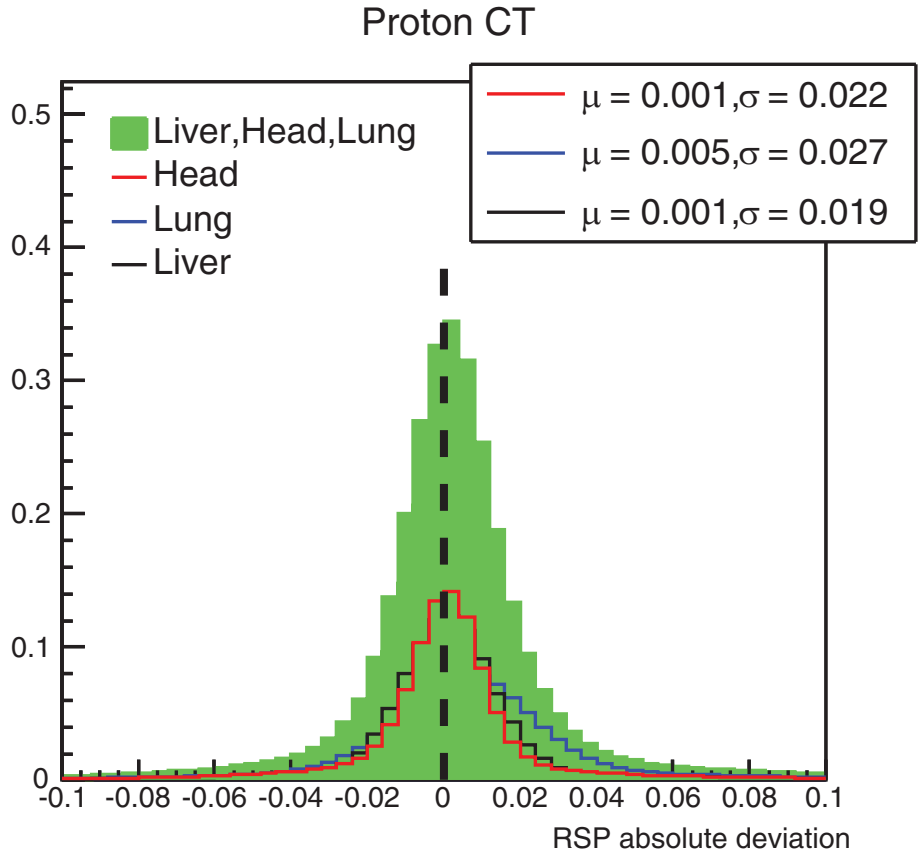

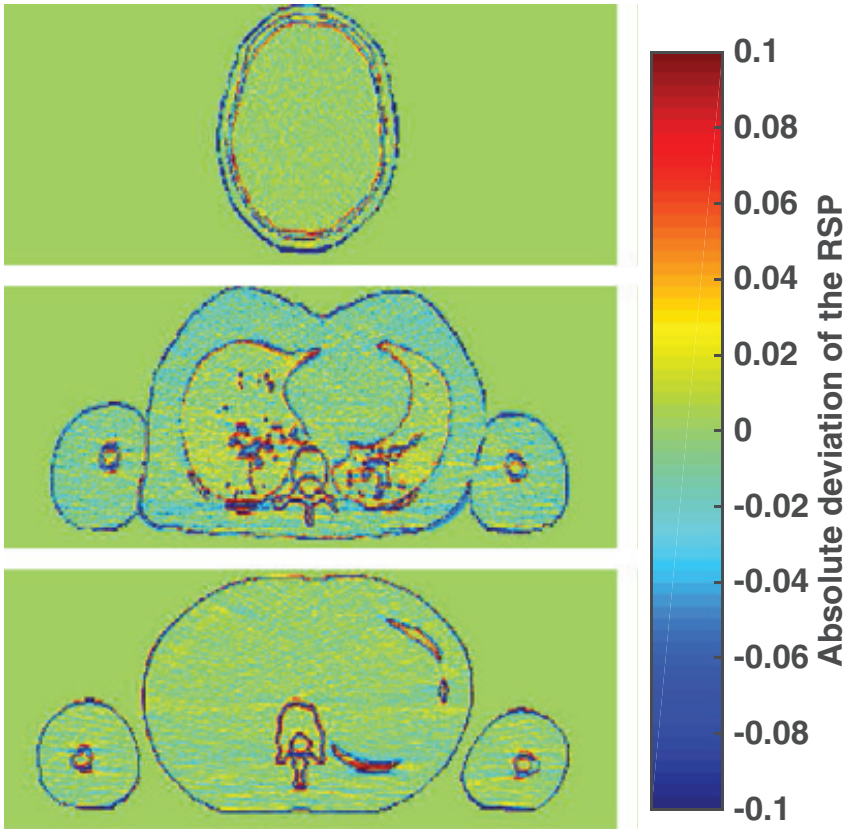

Deviation of the RSP wrt ICRP reference: high accuracy and a few % precision.

Estimation of the RED: projection-based DECT

[Alvarez and Macovski, 1976]

Initial decomposition

$$\mu(E) = \sum_j a_j f_j(E) = a_1 \underbrace{E^{-3}}_{\text{PhE}} + a_2 \underbrace{f_{\text{KN}}(E)}_{\text{Compton}}$$

$$a_1 \approx \frac{K_1 \rho Z^n}{A} = \frac{K_1 \rho_e Z^{n-1}}{N_A} \text{ with } n \approx 4 \quad \text{and} \quad a_2 \approx \frac{K_2 \rho Z}{A} = \frac{K_2 \rho_e}{N_A}$$

$\Longrightarrow$ Separable model in space and energy

$$\int_{s \in L(\boldsymbol{u},\theta)} \mu(\boldsymbol{x}(s), E)\, \mathrm{d}s = A_1(\boldsymbol{u},\theta) f_1(E) + A_2(\boldsymbol{u},\theta) f_2(E)$$

$$A_i(\boldsymbol{u},\theta) = \int_{s \in L(\boldsymbol{u},\theta)} a_i(\boldsymbol{x}(s))\, \mathrm{d}s$$

Estimation of the RED: projection-based DECT

[Alvarez and Macovski, 1976]

System of 2 equations with 2 unknowns A_1 and A_2:

$$I_1(A_1, A_2) = \int_{E \in \text{spectrum1}} S_1(E) \exp\left[-A_1 f_1(E) - A_2 f_2(E)\right] \mathrm{d}E$$

$$I_2(A_1, A_2) = \int_{E \in \text{spectrum2}} S_2(E) \exp\left[-A_1 f_1(E) - A_2 f_2(E)\right] \mathrm{d}E$$

- Inversion: Simplex, Polynomial model + calibration
- Reconstruction of each 3D material images

Separability model

$$\mu(m,E) \simeq \sum_{i\in\{\text{PhE},\text{CS}\}} f_i(m) g_i(E)$$

- Optimal f_1 and f_2 depend on the material set
- Separability in position and energy does not hold for a large spectrum range
- Sensitivity to scatter

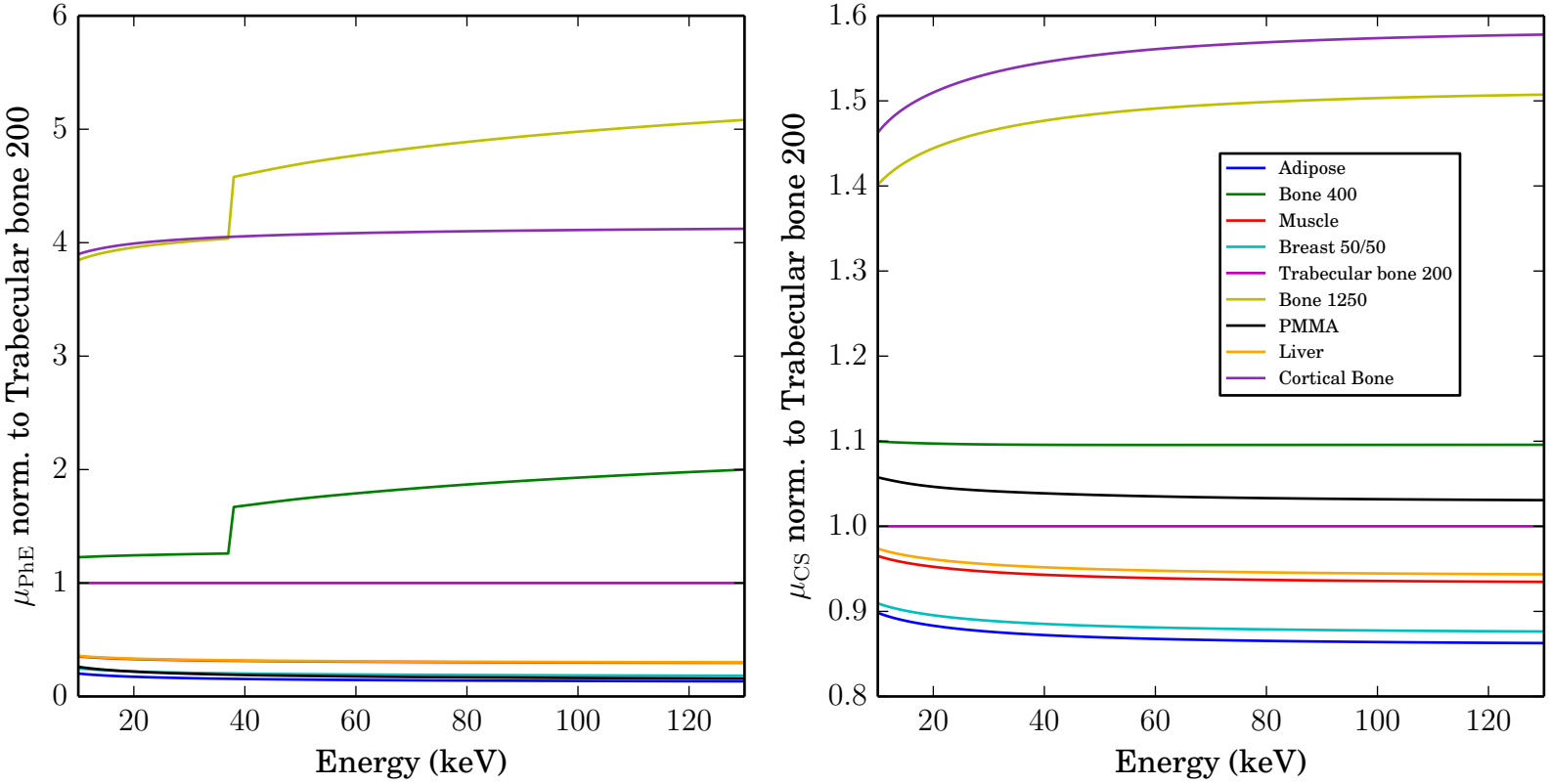

Estimation of the RED: accuracy

[Vilches-Freixas et al., 2016]

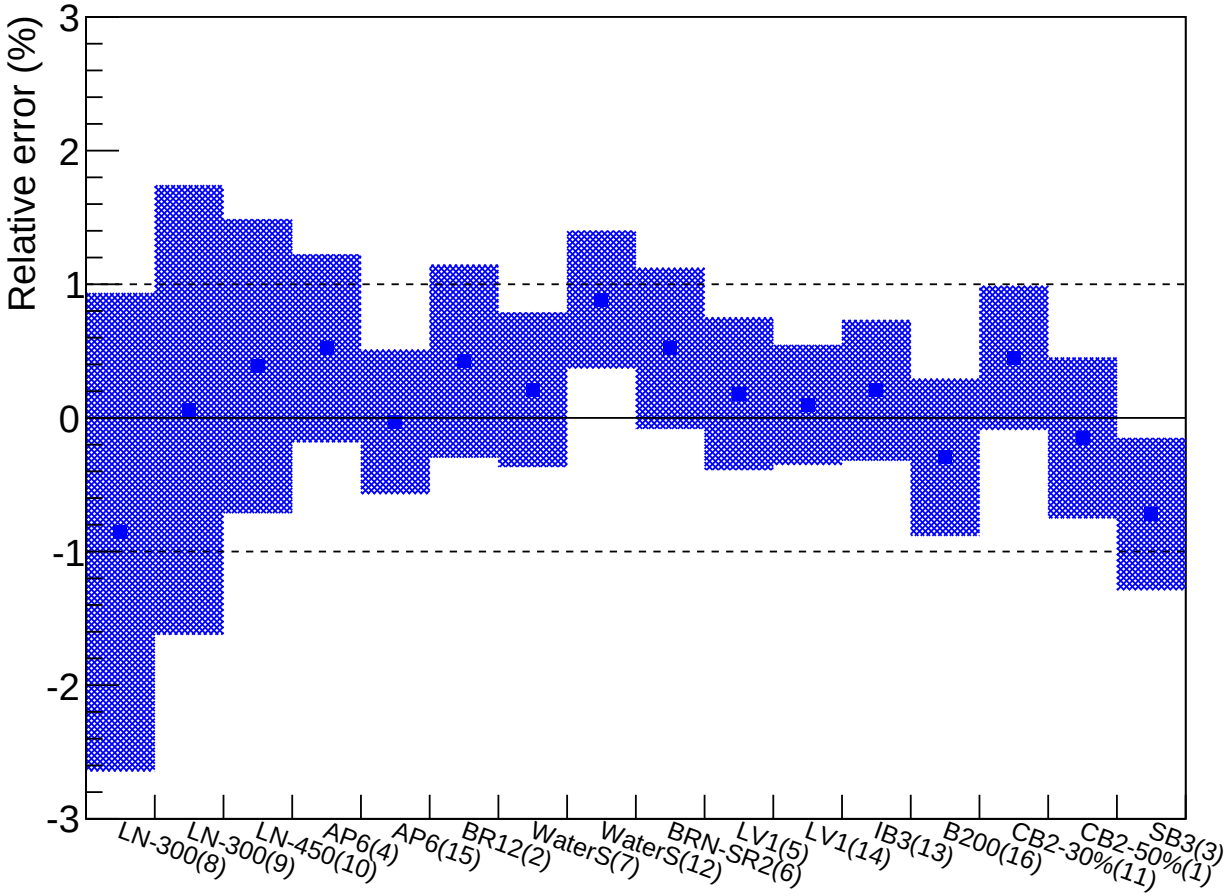

RED accuracy and precision results for each insert of the Gammex 467 phantom (78 kV, 94 kV, 0.1 mm Sn) for the 20 mGy acquisition.

Relative error analysis

$$I_m(\boldsymbol{x}) = \left(2m_e c^2 \beta^2 \gamma^2 \exp\left(-\beta^2\right)\right)^{1-r(\boldsymbol{x})} I_{\mathrm{w}}^{r(\boldsymbol{x})}$$

where

$$r(\boldsymbol{x}) = \frac{\mathrm{RSP}(\boldsymbol{x})}{\mathrm{RED}(\boldsymbol{x})}$$

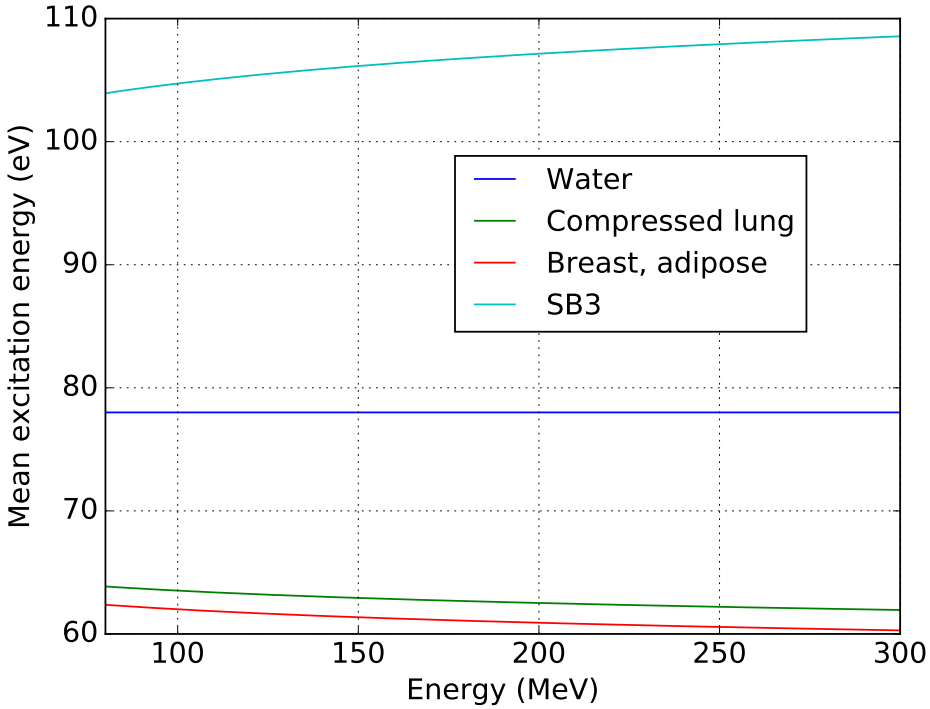

Dependence of a few % wrt the energy

$$\text{RelativeError}(I) = \underbrace{\left(\ln \frac{2 m_e c^2 \beta^2 \gamma^2 \exp\left(-\beta^2\right)}{I_w} \right)}_{\text{K} \approx 8.5} r \ \text{RelativeError}(r)$$

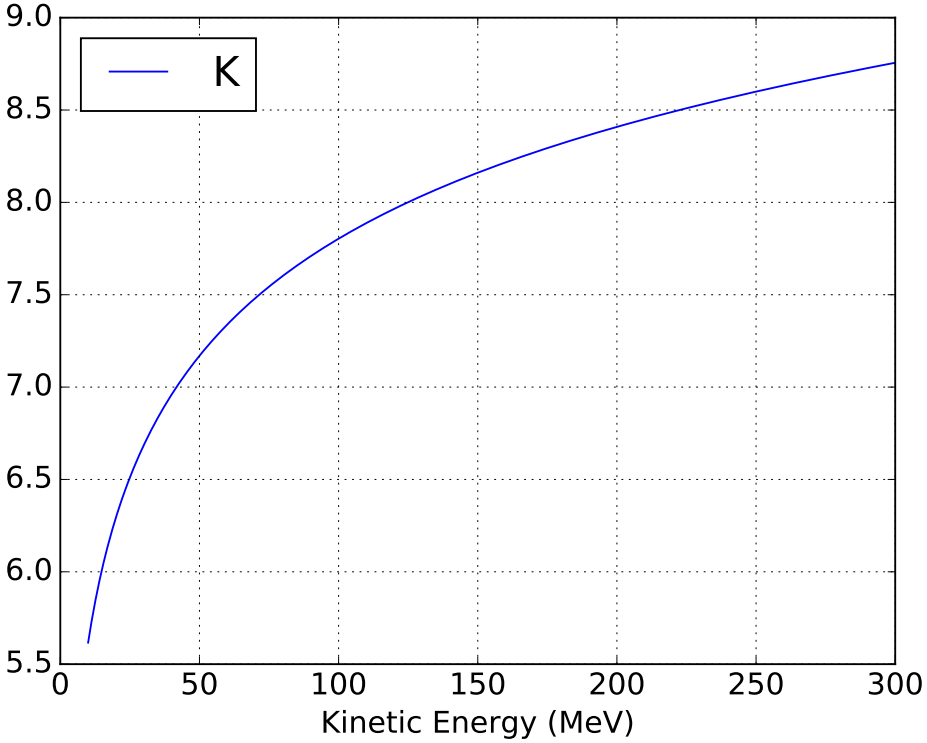

2% on both RED and RSP $\Longrightarrow$ 24% on I

Results: dose

[Arbor et al., 2015]

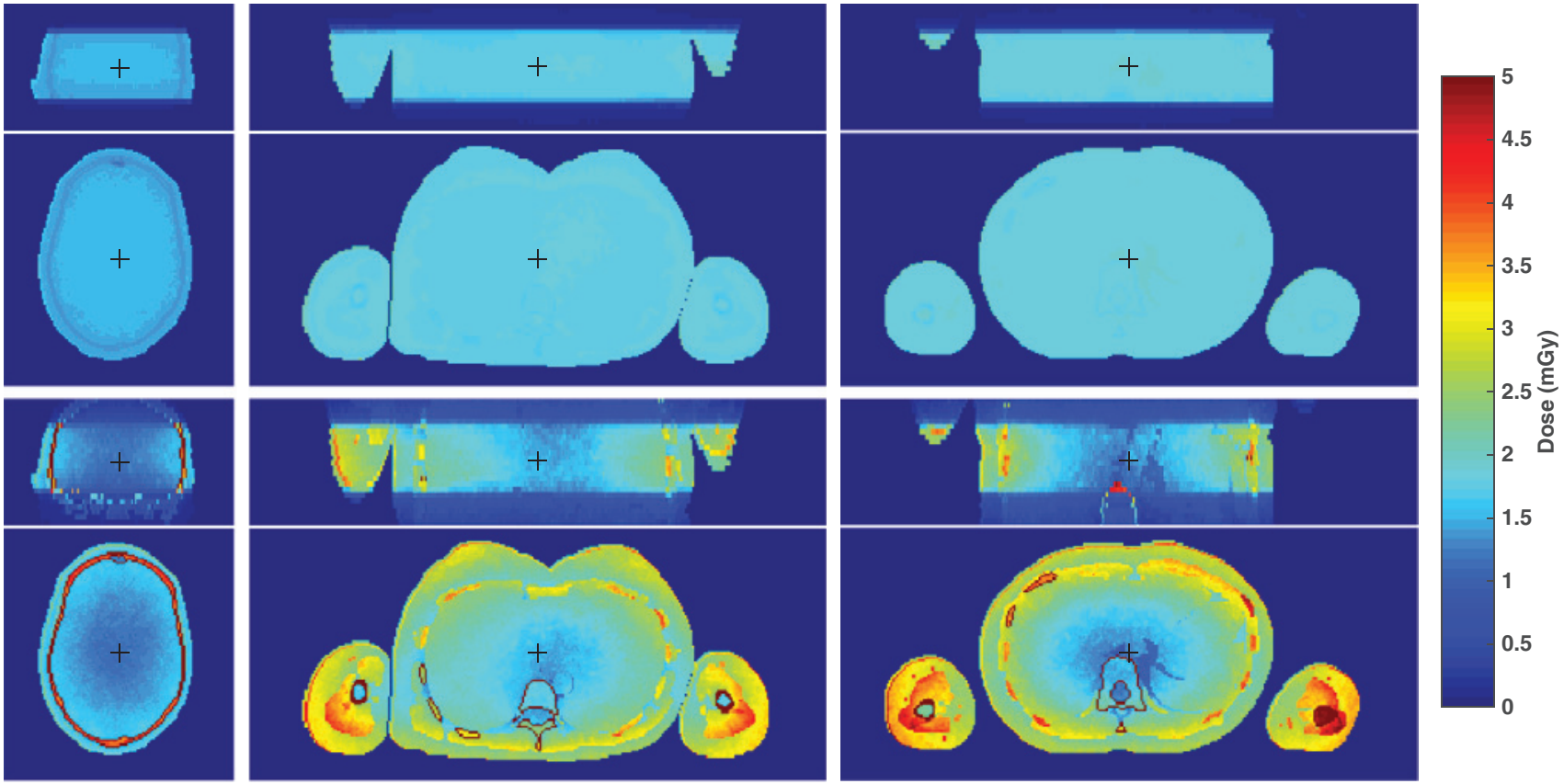

Spatial distribution of the dose delivered in pCT (top) and xCT (bottom)

Results

ICRP 110 phantom

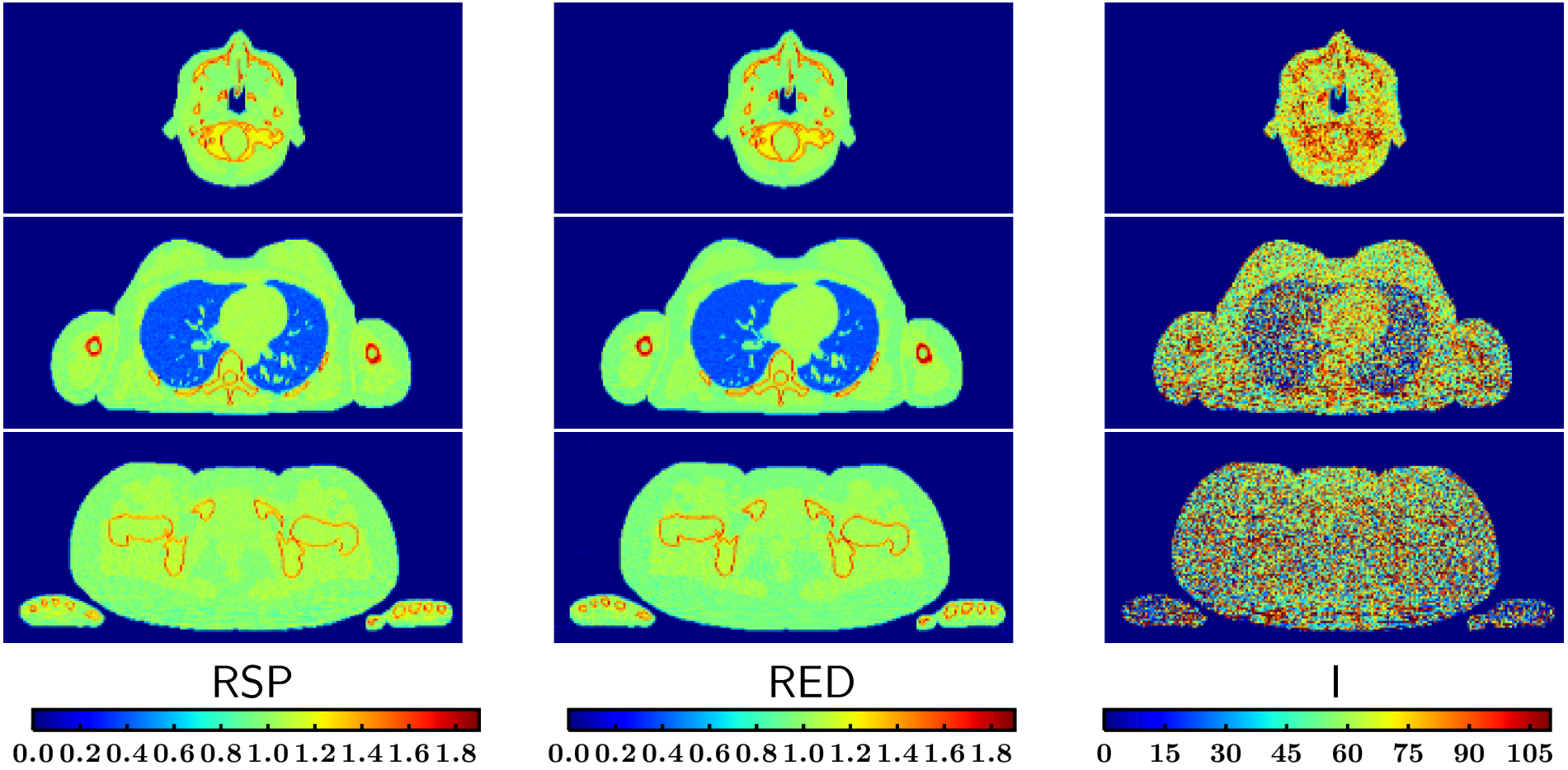

Results

ICRP 110 phantom

	ROI	Tissue	RED (unitless) Ref.	RED (unitless) $\mu \pm \sigma$	RSP (unitless) Ref.	RSP (unitless) $\mu \pm \sigma$	I (eV) Ref.	I (eV) Med $\pm\sigma$	σ_I (eV) theory	I error (%)
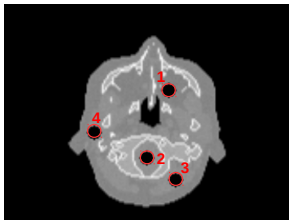	1	Adipose	0.95	0.95 $\pm$ 0.02	0.97	0.97 $\pm$ 0.02	63	60 $\pm$ 13	14	-5.0
	2	Brain	1.04	1.05 $\pm$ 0.02	1.06	1.06 $\pm$ 0.02	69	71 $\pm$ 20	17	3.0
	3	Muscle	1.04	1.04 $\pm$ 0.02	1.05	1.05 $\pm$ 0.02	69	74 $\pm$ 14	15	7.2
	4	Salivary gland	1.02	1.02 $\pm$ 0.02	1.04	1.04 $\pm$ 0.02	68	67 $\pm$ 13	15	-1.2
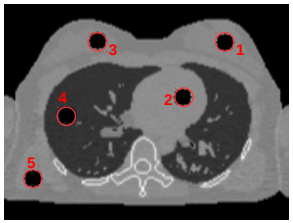	1	Mammary gland	1.02	1.02 $\pm$ 0.02	1.04	1.05 $\pm$ 0.02	64	62 $\pm$ 20	22	-3.1
	2	Blood	1.05	1.05 $\pm$ 0.02	1.06	1.06 $\pm$ 0.02	70	70 $\pm$ 24	21	0.8
	3	Mammary gland	1.02	1.02 $\pm$ 0.02	1.04	1.04 $\pm$ 0.02	64	65 $\pm$ 24	21	1.6
	4	Compressed lungs	0.38	0.38 $\pm$ 0.02	0.39	0.39 $\pm$ 0.02	70	54 $\pm$ 46	49	-21.8
	5	Muscle	1.04	1.03 $\pm$ 0.04	1.05	1.04 $\pm$ 0.04	69	65 $\pm$ 36	37	-6.9
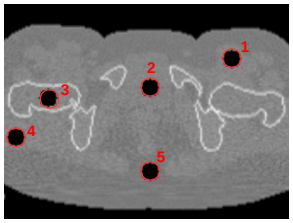	1	Muscle	1.04	1.04 $\pm$ 0.03	1.05	1.05 $\pm$ 0.03	69	67 $\pm$ 29	30	-2.9
	2	Urine	1.03	1.03 $\pm$ 0.05	1.05	1.04 $\pm$ 0.05	70	60 $\pm$ 37	33	-14.5
	3	Femora spongiosa	1.04	1.03 $\pm$ 0.05	1.06	1.05 $\pm$ 0.05	67	62 $\pm$ 39	36	-7.1
	4	Muscle	1.04	1.05 $\pm$ 0.05	1.05	1.06 $\pm$ 0.05	69	78 $\pm$ 38	47	12.3
	5	Adipose	0.95	0.95 $\pm$ 0.04	0.97	0.98 $\pm$ 0.04	63	59 $\pm$ 37	35	-6.5

I-value not a Gaussian distribution $\Rightarrow$ ROI median value

Conclusions

- Difficulty in estimating I-value for compounds
- Proposed method reached 15% accuracy for most anatomical sites
- Similar noise contributions (about 2%) for RSP and RED
  - RSP with 5 mGy pCT
  - RED with 20 mGy DECT
- Limitations: pCT with perfect detectors (energy and position)
- Application:
  - Intra-organ or intra-tissue variability of I-value
  - Build a database of different population groups (children/adult, male/female, ill/healthy...)

References

R E Alvarez and A Macovski. Energy-selective reconstructions in x-ray computerised tomography. *Phys Med Biol*, 21(5):733–744, September 1976. ISSN 00319155. doi: 10.1088/0031-9155/21/5/002.

N Arbor, D Dauvergne, G Dedes, JM Létang, K Parodi, CT Quiñones, E Testa, and S Rit. Monte carlo comparison of x-ray and proton CT for range calculations of proton therapy beams. *Physics in medicine and biology*, 60(19):7585, 2015.

A Besemer, H Paganetti, and B Bednarz. The clinical impact of uncertainties in the mean excitation energy of human tissues during proton therapy. *Physics in medicine and biology*, 58(4):887, 2013.

H Bethe. Zur Theorie des Durchgangs schneller Korpuskularstrahlen durch Materie. *Annalen der Physik*, 397(3):325–400, 1930. doi: 10.1002/andp.19303970303.

F Bloch. Zur Bremsung rasch bewegter Teilchen beim Durchgang durch Materie. *Annalen der Physik*, 408(3):285–320, 1933. doi: 10.1002/andp.19334080303.

P J Doolan, C-A Collins-Fekete, M F Dias, T A Ruggieri, D D'Souza, and J Seco. Inter-comparison of relative stopping power estimation models for proton therapy. *Physics in Medicine and Biology*, 61(22):8085–8104, oct 2016. doi: 10.1088/0031-9155/61/22/8085. URL http://dx.doi.org/10.1088/0031-9155/61/22/8085.

ICRU. Report no. 37: Stopping powers for electrons and positions. Technical report, International Commission in Radiation Units & Measurements, 1984.

ICRU. Report no. 49: Stopping powers and ranges for protons and alpha particles. Technical report, International Commission in Radiation Units & Measurements, 1993.

S Rit, R Clackdoyle, J Hoskovec, and J M Létang. List-mode proton CT reconstruction using their most likely paths via the finite Hilbert transform of the derivative of the backprojection. *Fully3D*, 2015.

J R Sabin, J Oddershede, and S P A Sauer. On the determination of the mean excitation energy of water. *Adv. Quantum Chem*, 65:39–62, 2013.

U Schneider, E Pedroni, and A Lomax. The calibration of CT hounsfield units for radiotherapy treatment planning. *Phys Med Biol*, 41(1):111–124, Jan 1996.

S M Seltzer and M J Berger. Evaluation of the collision stopping power of elements and compounds for electrons and positrons. *The International Journal of Applied Radiation and Isotopes*, 33(11):1189–1218, nov 1982. doi: 10.1016/0020-708x(82)90244-7.

M Tanabashi and PDG. Review of particle physics. *Physical Review D*, 98, 2018.

G Vilches-Freixas, J M Ltang, N Ducros, and S Rit. Dual-energy CT spectra optimization for proton treatment planning. In *4th International Conference on Image Formation in X-Ray Computed Tomography*, pages 585–588, 2016.

G Vilches-Freixas, C T Quiñones, J M Létang, and S Rit. Deriving the mean excitation energy map from dual-energy and proton computed tomography. *Physics and Imaging in Radiation Oncology*, 2018.